BNL 32212
Conf-821103--52

Physical Basis for Prompt-Neutron Activation Analysis

BNL--32212
DE83 003938

Robert E. Chrien

Brookhaven National Laboratory

Upton, New York, 11973

(516) 282-3903

Total number of pages:

Outline:

I. Introduction: Statement of the Technique

II. Instrumentation and Sources

III. Physics of Electromagnetic Interaction

IV. Thermal, Resonance and Broad Range Energy Capture

V. Systematics: Photon and Neutron Strengths

VI. Fast Neutron Capture

I. Introduction

In recent years the usefulness of the technique called "prompt γ-ray neutron activation analysis" has been established in a wide range of application to rapid materials analysis, as exemplified in the accompanying papers in this symposium. The term prompt γ-ray neutron activation is to be understood as the observation of the characteristic electromagnetic radiation generated by the neutron radiative capture. This radiation is prompt in the sense that the nuclear decay time is in the order of $h/\Gamma \approx 10^{-15}$ sec and thus strongly contrasts with the time delay of seconds, or longer, characteristic of β-delayed γ-radiation. Hereafter I shall avoid the use of the term "activation", which is not strictly applicable here, and refer to the applications of radiation neutron capture spectroscopy or neutron capture γ-ray spectroscopy. As is shown in figure 1, the prompt γ rays include also those from inelastic neutron scattering. Since the threshold for these is determined by the position of the first excited state of the target, they are of interest only when fast neutrons are used.

The topic of radiative neutron capture is virtually as old as the discovery of the neutron itself. Within a year after Chadwick's great discovery, one of his students, D. E. Lea, had observed γ rays resulting from the bombardment of paraffin from a polonium-beryllium neutron source. These could be attributed to the capture of neutrons by protons and he estimated the size of the capture cross section. It is interesting to note that his cross section estimate was about a thousand times larger than one inferred from Goldhaber and Chadwick's experiment on the photodisintegration of the deuteron. Goldhaber (1) relates that he suggested to Chadwick that the reason for the discrepancy might be that the neutrons were slowed down by the paraffin before capture; Chadwick advised against publishing this notion, saying that at the Cavendish, speculation in publication was discouraged. It was only 3 months later that

Fermi reported the discovery of slow neutrons. In a very few months Fermi and his co-workers established the most important experimental facts about slow neutron capture. These facts led directly to Bohr's enunciation of the theory of the compound nucleus, laying the foundations of nuclear physics.

These early experiments were performed with very crude instrumentation. The photon energies, for example, were inferred from absorption measurements in lead and other materials. The wealth of information contained in the frequency distribution of the electromagnetic radiation was largely concealed from these pioneers. Furthermore, the isotomic neutron sources used--typically (α-n) or ^{9}Be, were woefully weak by modern standards. The strongest such source was employed by Jobot and Curie (2), who had 700 mCi of polonium--a source yielding about 10^{6} n/sec over a 4π solid angle.

II. Sources and Detectors

The birth of neutron capture γ-ray spectroscopy had to await the availability of the modern research reactor. These appeared, both in the East and West, shortly after the Second World War, providing fluxes of 10^{13}n/cm^2/sec and external particle currents of $\approx 10^{9}$ n/cm^2/sec. These sources made the use of high resolution detectors possible. Early pioneers in this field include Groshev and collaborators (3) and Kinsey and Bartholomew (4) who employed magnetic spectrometers with a resolution of a few parts in a thousand. Bent crystal spectrometers with much higher resolutions were subsequently employed, particularly at low photon energies. More recently bent crystal spectrometers have been used with internal targets, such as those at the ILL, Grenoble, so that the inherently low efficiency of these devices can be overcome, while maintaining their excellent resolution. At high photon energies, the use of semiconductor diodes of rather large size has become popular since these combine high efficiency with superior resolution.

Figure 3 depicts the resolution available at the modern bent crystal spectrometers at the ILL, Grenoble, and that available with a germanium detector. For GAMS 1 at ILL a resolution of 8 eV at 100 keV is achievable in 5th order reflection. For germanium a resolution of about 5 keV at 8 MeV is achievable with relatively high efficiency. For commercial applications, the high sensibility and portability of the intrinsic germanium detector makes it the instrument of choice, especially when modest neutron source strengths are employed.

III. The Theory of Radiative Capture

What is the nature of this (n,γ) reaction whose spectrum is such a distinct signature of the target isotope? For a consideration of this question, a brief review of the fundamental properties is presented.

Early reaction theories dealt only with particle channels. Lane and Thomas (5) showed that perturbation theory can be employed to place photons on an equivalent (but not identical) basis to particle channels in R-matrix theory.

The radiative transition probability T between a resonance λ in state ψ and final state Φ is given by the perturbation theory expression (6):

$$T = \frac{2\pi d\rho}{\hbar} \left|\langle\psi\left|H'(A)\right|\Phi\rangle\right|^2 \qquad (1)$$

where H'(A) is the electromagnetic perturbation operator written in terms of the vector potential A, and dρ is the density of photon states within the solid angle dΩ.

The photon width amplitude is related to the electromagnetic perturbation operator:

$$e^{i\phi_\gamma}\Gamma_{\lambda\gamma}^{1/2} = \left(\frac{2\pi d\rho}{\hbar}\right)^{1/2} \hbar^{1/2} \int d\tau X_\lambda^* H'(A)\Phi \qquad (2)$$

At this point a difference between particle and photon channels becomes apparent. In R-matrix theory the states X_λ are defined only for the internal region of configuration space; for photons there can be a sizable contribution to the photon width amplitude from the external, $r>a_c$, region. This external region contains both resonance and non-resonance components of the wave function, and the collision matrix, U may be decomposed as follows:

$$U = U_{Res} + U_{POT}$$

and

$$U_{Res} = U(\text{internal}) + U(\text{external})$$

where U_{POT} results from the position of the neutron wave scattered by the surface of the nucleus--the so-called potential scattering. This latter term may further be decomposed into hard sphere and distant resonance contributions. The collision matrix also includes contributions from both open and closed channels in the external region. Figure 4 summarizes the various reaction mechanisms in terms of a hierarchy of excitations of increasing intensity.

The form of the interaction operator is taken from classical electromagnetic theory (7):

$$H'(\underline{A}) = (4AM_c)^{-1} \sum_{j,k} \left\{\underline{P}_j - \underline{P}_k - \frac{e_j}{c}\underline{A}(r_j) + \frac{e_k}{c}\underline{A}(r_k)\right\}^2$$

$$+ V' - \left(\frac{e\hbar}{2Mc}\right) \sum_j \mu_j (\underline{\sigma}_j \cdot \text{curl } \underline{A}_j) \qquad (3)$$

This operator is linearized by dropping terms of the order of A^2 which is equivalent to consider the interaction in terms of a single photon; the last term above describes the interaction of the intrinsic magnetic moments of the nucleus. The electromagnetic field is expended into its various multipoles and the multipoles can be divided into two groups.

(a) parity $(-)^L$; these are electric multipole operators (because they arise mainly from the charge terms);

(b) parity $(-)^{L+1}$; magnetic multipole operators (because of the contribution from the magnetic moments).

The components of the electromagnetic perturbation operator are proportional to irreducible tensor operators denoted by H_{TM} where T denotes the parity.

Thus the partial radiation amplitude for a photon channel with multipolarity LM (in which the photon carries L units of angular momentum and M units of angular momentum projection on the z axis) is

$$\Gamma^{1/2}_{\lambda(\gamma LM)} = \frac{(8\pi)^{1/2} k_\gamma^{L+1/2} (L+1)^{1/2}}{L^{1/2}(2L+1)!!} \langle X^{\ell}_{\lambda Jm} | H^{L}_{TM} | \phi_{\mu J'm'} \rangle \qquad (4)$$

for the transition from a state λ with angular momentum J and z-projection m to a final state μ with angular momentum J' and projection m'.

In M^{th} component $H^L{}_{TM}$ the general subscript T has to be specialized to either electric or magnetic radiation according to the parity difference $(-1)^L$ or $(-1)^{L+1}$ respectively, of the initial or final state.

In the long wave length approximation ($k_\gamma a \ll 1$), forms of the operator $H^L{}_{TM}$ for E1 and M1 transitions (for $E_\gamma < 10$ MeV) are

$$H'_{E1} = \sum_k e_k r_k Y^1_\mu(\theta_k, \phi_k)$$

$$H'_{M1} = \frac{e\hbar}{2Mc} \left(\frac{3}{4\pi} \right)^{1/2} \sum_k (L_{kM} + \mu_k \sigma_{kM}) \tag{5}$$

These amplitudes are the only multipoles of significance for neutron capture. Measurable E2's are quite rare and no other multipoles have been observed. Note that the M1 expression contains contributions for the orbital and spin angular momentum components.

What prescriptions can we provide for calculation of these radiative widths? Only a few simple models are available to us.

One prescription is to assume the statistical model, namely Bohr's compound nucleus model. The reaction cross section is expressed in terms of the collision matrix $U_{cc'}$ which contains the R-matrix expression,

$$R_{cc'} = \frac{\gamma_{\lambda c}\gamma_{\lambda c'}}{E_\lambda - E} \tag{6}$$

The resonance wave function $|\lambda\rangle$ is expected to be complicated, with only a small overlap with the channel functions, i.e., $\langle\lambda_c\rangle^2 \approx 10^{-4}$ to 10^{-7}. In this approximation, the $\gamma_{\lambda c}$ can be considered as a random variable.

The fundamental assumptions of the statistical model are:

(a) $\gamma_{\lambda c}$ and $\gamma_{\lambda c'}$ have random signs such that $\sum_{\lambda_{c \neq c'}} \gamma_{\lambda c}\gamma_{\lambda c'} = 0$.

(b) $\gamma_{\lambda c}$ and $\gamma_{\lambda c'}$ are independent and uncorrelated such that the linear correlation coefficient is zero, i.e., $\rho(\gamma_{\lambda c}, \gamma_{\lambda c'}) = 0$.

(c) The strength function for channel c is independent of energy over the range ΔE, i.e., $1/\Delta E \; \Sigma_\lambda \; \gamma^2_{\lambda c}$ = constant.

Because $\gamma_{\lambda c}$ is the coupling amplitude of entrance channel c with the resonance state at energy E_λ, the above assumptions imply that the statistical properties of the exit channel c' contain no 'memory' of the entrance channel amplitude.

To evaluate the partial radiative width, under these assumptions, one can adopt the "black" nucleus picture of Blatt & Weisskopf (8); for a spinless particle in a bound S-state, the El transition width to a low-lying P state is

$$\Gamma_{s\gamma p} = \frac{16\pi k_\gamma^3}{9} \left|\langle J=0 \left|\left| Y^1 \right|\right| J=1\rangle\right| \left\{\langle e\rangle \int_o^\infty dr\ r\ u_0(r) u_1(r)\right\}^2 \qquad (7)$$

where $\langle e\rangle$ is the effective charge of a particle in a system of particles (for a neutron $\langle e\rangle = (-Z/A)e$; proton $\langle e\rangle = (N/A)e$). The photon wave number is $k_\gamma = E_\gamma/hc$.

In the statistical model the initial single particle state is dissolved among the compound nucleus states over an energy interval corresponding to the spacing of the single particle states D_s.

If the radial wave functions are assumed uniform within the nuclear radius (a) and zero outside, an estimate of the integral above is

$$\int_o^\infty dr\ r\ u_0(r) u_1(r) = 3a/4\ ; \qquad (8)$$

$$\text{hence} \quad \Gamma_{\lambda\gamma p} \approx 3/4\ \langle e^2\rangle\ (E\gamma/\hbar c)^3\ a^2\ \langle D_o\rangle/D_s$$

for an S→P transition. The width is further fragmented among the final P-states available. The estimate for $\Gamma_{S\gamma P}$ is understood as an <u>average</u>

value. The specific values will fluctuate about the mean and that fluctuation is describable by the Porter-Thomas distribution--i.e., a chi-square distribution with one degree of freedom (8). The primary γ-ray intensity for E1's by multiplying by the level density of the p-wave final states:

$$f_1(E)dE = 3/4 \langle e^2 \rangle (E\gamma/\hbar c)^3 a^2 \rho \frac{(E_{th}-E_\gamma)}{\rho(E_{th})} \frac{dE_\gamma}{D_S} \qquad (9)$$

This spectrum is not directly observable because of this presence of secondary and higher order cascade γ rays. Figure 5 shows an observed spectrum, taken with the Compton spectrometer of Groshev, for elemental samarium. This figure is shown to give an overall view of the capture spectrum, which shows resolved cascade γ rays at low energies and resolved primary lines at high energies, and an unresolved continuum in the middle.

IV. Non-statistical Capture

The statistical assumption is known to fail in cases where the reduced neutron widths are large, and insufficient fragmentation of the single particle strength occurs. In such cases the external part of the matrix element dominates, and we have the situation known as channel or valence capture. In that case the γ-ray widths are fully correlated with the final and initial state reduced widths (9),

$$\Gamma_{\lambda\mu}(Ch) = \frac{16\pi}{9} k_\gamma^3 (2/a)^2 \theta_\mu^2 \theta_\lambda^2 (\langle e \rangle a/k_\mu)^2 \frac{\langle J_\lambda || Y^{(1)} || J_\mu \rangle^2}{2J_\lambda+1} \qquad (10)$$

A direct reaction mechanism can also occur in non-resonant capture; the simplest example being that of hard sphere capture. Here the final state wave funtion corresponds to scattering from an impenetrable sphere, and the cross section can be shown to be

$$\sigma_{\gamma\mu}(HS) = \frac{0.062}{a\sqrt{E_n}} \cdot \left(\frac{Z}{A}\right)^2 \cdot \theta_\mu^2 y^2 \left(\frac{y+3}{y+1}\right)^2 \qquad (11)$$

where E_n is the neutron energy in eV, a is the nuclear radius in fm; $y = k_\mu a$ and k_μ is the neutron wave number for the single particle state bound by energy E_γ, defined above.

The hard sphere cross section is proportional to y^2 or E_γ. Since this cross section is proportional to

$$k_\gamma^3 [\langle \theta_\lambda || D || \theta_\mu \rangle]^2 \ , \qquad (12)$$

the dipole matrix element must be proportional to E^{-1}.

Kopecky et al. (10) have shown that direct capture occurs in the 3s region at thermal energies. The final state correlations between the (n,γ) and (d,p) cross sections are greatly improved by the use of an E_γ energy dependence for the radiative strength, rather than the usual E_γ^3 factor, when nearby resonances have no influence on the cross section.

The direct capture effect can be seen most clearly for thermal neutron capture, in those cases where no nearby resonances influence the cross section. As shown in figure 6 for ^{130}Te, the spectrum for E1 radiation can be well predicted once the spectroscopic factors for single neutron transfer are known (11).

V. The Giant Dipole Resonance

For most heavy nuclides, however, the statistical model works well. The average photon strengths, however, do not exhibit the E^3 dependence of the Weisskopf estimates, which are based on a single particle model. The fact is that collective nuclear motions exert a profound effect on the strength distribution. It is well known that the E_1 strengths are concentrated in nuclei in the energy region of the giant dipole resonance.

The photoexcitation cross section may be directly related to the photon strength function, $\langle\Gamma\rangle/D$,

$$\frac{\langle\Gamma_{\gamma\mu}(E_\gamma,J_\mu)}{D(J_\mu)} = \frac{4}{3\pi}\ \frac{NZ}{A}\ \frac{e^2}{\hbar c}\ \frac{(1+0.8x)}{M_c^2}\ \frac{(\Gamma_G E_\gamma)^2}{(E_\gamma^2-E_G^2)^2+\Gamma_G^2E_G^2} \qquad (13)$$

This expression can be expanded in a power law around the position of the neutron binding energy. Axel first wrote the resulting expression, valid near A=100 and E_γ=7 MeV (12)

$$\frac{\Gamma_{\gamma\mu}}{D} = 2.2\times10^{-5}\ \left(\frac{E}{7\ \text{MeV}}\right)^5\ \left(\frac{A}{100}\right)\ \left(\frac{\Gamma_G}{5}\right) \qquad (14)$$

While this expression is valid only for transitions to the ground state, it can be applied from transitions to excited states by assuming Brink's hypothesis, that a giant resonance can be built in each excited state of the nucleus (13). The variation of radiative widths has been studied, for example, for ^{196}Pt, and the results shown in figure 7 are in good agreement with the Brink-Axel hypothesis. Then we can define an expression for the photon strength function with the energy and A dependence factored out,

$$S(E1) = \langle \Gamma_{\lambda\gamma\mu} \rangle \, [D_\lambda E_\gamma^5 A^{8/3}]^{-1}$$

$$= 6.1 \times 10^{-15} \text{ MeV}^{-5} \qquad (14)$$

This expression can be contrasted to Weisskopf's single particle estimate for E1 radiation,

$$\frac{\Gamma_{\lambda\gamma\mu(E1)}}{D_\lambda} = 6.8 \times 10^{-8} \, E_\gamma^3 \, A^{2/3} \, D^{-1} \approx 3 \times 10^{-9} \, E_\gamma^3 \, A^{2/3} \qquad (14)$$

The parameter D refers to the final state spacing for levels which can combine with the capture state levels through E1 transitions. A value of D≈20 MeV is obtained experimentally by treating it as a fitted parameter.

The Weisskopf single particle model (SPM) predicts an $A^{2/3}$ dependence and the Axel GDR parameterization an $A^{8/3}$ dependene of the E1 strength function. A compilation of the dependence of E1 strengths has been presented by McCullagh, Stelts and Chrien (14). Results from (n,γ), (γ,n) and (γ,γ') measurements on discrete resonances were examined for about 50 data sets, with renormalization of some results to more recent values of absolute partial widths. The E1 A-dependence is compared to the predictions of the SPM and GDR. Results for the latter are shown in figure 8 where the solid and dashed lines indicate the unweighted average value and the Axel GDR prediction. (Note (γ,γ') data are not included in the average because of their poor statistical accuracy.) Errors reflect the number of transitions contributing to each datum point.

The average ratio of observed and GDR strength functions is 0.69 ± 0.06,

indicating that the GDR calculation overestimates the experimental data by about 30%.

This fact has been attributed by Gardner and Gardner (15) to a modification of the Lorentzian function, which they claim is not an adequate representation of the giant resonance in the tail region. They suggest using a modified Breit-Wigner form which in fact fits the data much better, and provide some theoretical justification on the basis of the availability of particle-hole states into which the giant resonance can be fragmented.

The situation for M1 giant resonance influences on the observed M1 strengths in nuclei is far from clear, both experimentally and theoretically.

The single particle estimate is as follows:

$$\frac{\Gamma_{\lambda\gamma\mu}(M1)}{D_\lambda} = 2.1 \times 10^{-8} E_\gamma^3 D^{-1} \qquad (16)$$

$$\approx 18 \times 10^{-9} E_\gamma^3$$

from experimentally observed M1 transitions.

It is generally assumed, for nuclides with $A \geq 100$, that the M1 and E1 transitions have the same energy dependence and that there is a constant ratio of 7 ± 1 for $\langle E1 \rangle / \langle M1 \rangle$. There is no justification for this assumption, which in any case is applied to such a limited energy range that the energy dependence does not much matter. Recent experiments have been carried out over a wide enough energy range so that the different energy dependences are revealed. Figure 9 shows the results for ^{239}Pu, as obtained using a transmission filtered beam of neutrons at 2 keV from the HFBR. Here the positive and negative parity

final states are clearly distinguished; the former are fed primarily by M1 transitions after S-wave capture, while the latter are fed by E1's. Even at 2 keV, however, the amount of p-wave capture is not negligible and must be factored in.

The results show in fact that the energy dependence for E1 and M1 widths must be quite different. While E1's widths vary with excitation energy as E^5_γ, due to the giant dipole resonance, the M1 transitions do not depend so markedly on energy. The variation seems to be consistent, after correction for P-wave effects, with the E^3 variation expected from Weisskopf estimates. Evidence for collective enhancement of M1 strengths in neutron capture is not convincing.

VI. Fast Neutron Capture

Above about 1 MeV, the cross sections predicted by the compound nucleus hypothesis model are inadequate to explain the experimental data. The importance of direct excitations relative to compound nucleus formation becomes more and more important with increasing neutron energy. The best example is direct capture of a neutron into a single-particle orbit. We describe it as a one-step reaction leaving the other nucleons unperturbed. Another example is the direct excitation of the giant dipole state caused by the incident neutron, which at the same time is inelastically scattered into a bound single-particle orbit. In the next step, the giant dipole may deexcite by the emission of γ-rays. This reaction is called "semidirect". It turns out that direct and semidirect reactions play a dominating role at neutron energies higher than about 5 MeV (15).

The direct and the compound nucleus models represent the extremes on the reaction-time scale. It is the essence of the CN model that the energy of the incident neutron be distributed over the nuclear volume. The direct mechanisms

involve the concentration on a single nucleon, or at least a limited region of the nuclear volume.

Thus direct processes are "fast" and are associated with the wide structures such as giant resonances.

The giant dipole state plays a dominating role in capture cross sections above 5 MeV. It is well known that there is an isospin dependence in the neutron-nucleus interaction. The force between the target protons and incident neutron is somewhat stronger than that between the target neutrons and the incident neutron. The result of this difference is expressed in the Lane potential term in the optical model:

$$V = V_0 + (V_1/A)\ \vec{t} \cdot \vec{T} \qquad (17)$$

where $\underline{t}$ is the nucleon isospin and T_{A-1} the isospin of the rest of the nucleus. The first term is the usual central potential and the second is referred to as the symmetry or isospin term. V_0 and V_1 are the depths of the potentials which often are assumed to have the same radial dependence (Woods-Saxon form).

In the case where the nucleus is in the ground state, $\underline{t} \cdot \underline{T}_{A-1}$ can be replaced by $1/2\ t_z\ (N-Z)$ and one gets

$$V = V_o + \frac{1}{2}\, t_z\, \frac{N-Z}{A}\ V_1 \qquad (18)$$

The size of V_1 can be inferred from the symmetry energy term in the semi-empirical mass formula, and it is approximately 100 MeV. For a heavy nucleus like Pb, the size of the polarizing term in the potential is about $1/11(44)100 \approx 5$ MeV (16).

To see the effect of the symmetry potential, let us consider nucleon capture. The nucleon, in addition to the (isoscalar) potential V_0, is subject to a potential $NV_1/4A$ from the N target neutrons and $ZV_1/4A$ from the Z protons and these potentials have opposite signs. An incident neutron, for example, will by the action of the symmetry potential repel the N neutrons and attract the Z protons. Hence, there will be a polarizing force between the neutrons and the protons of the target nucleus as the incident nucleon approaches the nucleus. The force is parallel to the force on the incident nucleon.

In nucleon capture, the symmetry potential is responsible for exciting simple, collective modes of motion in which the neutrons and protons move in opposite phases. The most important of these isovector (T=1) motions is the giant dipole resonance.

The cross section for this process is the square of an amplitude which has two terms: the first is just the direct term, the second is due to the polarizing action of the symmetry potential (17):

$$\sigma(j_i,j) = \left(\frac{8\pi}{9}\right)\left(\frac{\mu k_\gamma^3}{h^2 k_n}\right) \left|T_d(j_i,j) + T_{sd}(j_i,j)\right|^2 \qquad (19)$$

for the capture of an incident neutron with quantum numbers $l_i j_i$ into a bound single particle orbit with quantum numbers, n,ℓ,j, and the emissio of an E1 photon.

The contribution to the matrix elements T_d and T_{sd} may be written in terms of angular and radial components.

The radial components are given by

$$T \propto \langle R_{n\ell j} | 0 | R_{\ell_i j_i} \rangle \tag{20}$$

and for T_d, $0 = r$

for T_{sd}, $0 = rU_1(r)$

where $U_1(r)$ is the symmetry potential.

These two components, the direct and semi-direct term interfere destructively below the GDR and constructively above it. Figure 10 shows the predicted shapes calculated for ^{208}Pb.

Experimental observations so far have roughly confirmed the behavior of the fast capture cross section as outlined above, but with one major deficiency. That deficiency is the failure of the model to describe accurately the region of destructive interference below the resonance peak. Furthermore the model predictions are sensitive to the form of the optical potentials used to describe the interaction. There is also evidence that the symmetry potential must, in the general case, be assumed to be complex. A reasonable agreement with experimental data is achieved only if the following assumption is made for the form of the symmetry potential (18):

$$U_1(r) = Vf(r) - iW4a\ df/dr \tag{21}$$

$$\text{with } f = (1 - \exp\ (r-R/a))^{-1}$$

The results can be compared to experiment satisfactorily as shown in figure 11.

Three of the partial cross sections for neutron capture in ^{208}Pb are shown in fig. 11, namely for the $g_{9/2}$ ground state, the $i_{11/2}$ first excited state and the $g_{7/2} + d_{3/2}$ states at 2.49 and 2.54 MeV, respectively. All of them exhibit the resonance structure predicted by the direct-semidirect model. It was noted in the preceding section that the cross section for ground state γ rays in ^{209}Pb would be expected to have its maximum at $E_n = 9.5$ MeV. The cross section for capture into each of the other single-particle states should peak at a neutron energy shifted upwards by the excitation energy of the state. Thus, we would expect the maximum cross-section for the $i_{11/2}$ state to occur at $E_n = 10.3$ MeV and for the $g_{7/2} + d_{3/2}$ states at $E_n = 12.0$ MeV. The results are compatible with the Brink hypothesis (13) which prescribes that a giant dipole resonance is built on each excited state and that it has the same shape and magnitude as the one built on the ground state. The present results show that this is valid for the neutron single-particle states in ^{209}Pb.

Comparison with theoretical predictions for neutron capture by ^{208}Pb was first made with a surface-peaked coupling function (17). We show in fig. 12 the direct-semidirect cross section obtained with this coupling function and a strength $V_1 = 160$ MeV of the symmetry potential (solid curves). Despite the rather high strength value, the calculated cross sections are too low and, furthermore, there is a disturbing discrepancy in the neutron energy dependences. A much better description of the data is obtained with a complex coupling function. The results (dashed curves) are taken from a calculation (18) with $V_1 = 70$ MeV and $W_1 = 140$ MeV.

The physical significance of an imaginary term in the coupling between the direct and semi-direct reaction mechanisms is somewhat controversial. It may be understood, perhaps, as this excitation of the GDR oscillations through more

complicated reaction mechanisms than the simple polarization effect provided by the real term.

VII. Properties of Thermal Neutron Capture γ-ray Spectra

It should be evident from the summary presented above that only in a few isolated instances can thermal neutron capture γ-ray spectra be calculated from a model. We have seen that "hard sphere" capture results in a cross section of the order of a barn at thermal energies. If we have a cross section either significantly higher or significantly lower than a barn, we can be sure that a reaction mechanism other than hard sphere capture is present.

The most likely occurrence is the presence of a much larger cross section due to a nearby resonance. In this case one should expect a purely statistical reaction mechanism, since we know that in resonances, the compound nucleus hypothesis demands a complex and many component wave function. Thus the overlap between the initial and final states can be regarded in light of the central limit theorem of statistics. In this theorem, the sum of many small, uncorrelated, contributions or arbitrary phase will tend toward a variable with a Gaussian distribution with zero mean. If several distinct resonances contribute to thermal capture, the capture amplitude can be represented as the sum of Gaussian terms. In either case, whther single or multiple contributions, a Gaussian reduced width amplitude will result, and the square of that amplitude will result in a distribution, known as the Porter-Thomas distribution (8),

$$P(x) = \Gamma\ (1/2)^{-1}\ (x/2)^{-1/2}\ \exp\ \{-x/2\} \tag{20}$$

where $x = \Gamma/\langle\Gamma\rangle$

The consequences of the Porter-Thomas distribution are visualized from figure 13. The Porter-Thomas distribution is a member of the chi-square class of functions with one degree of freedom. The sum of several such distributions, of equal means, will result in a member of the chi-square class with the number of degrees of freedom equal to the sum of the several constituents. The behavior of the chi-square distribution is seen in the figure. For $\nu=1$ the most probable width is zero and the probability density function (but not its integral) diverges as $x = (\Gamma/\langle\Gamma\rangle) \rightarrow$ zero.

Thus γ-ray spectra from individual resonances, or thermal capture spectra where resonance tails dominate the cross section, will show this Porter-Thomas fluctuation. Where several spin values, $I\pm1/2$ for $\ell=0$, contribute due to a non-zero target spin, the distribution will be between $\nu=1$ and $\nu=2$ (an exponential distribution) depending on the relative contributions for the $I+1/2$ and $I-1/2$ spins.

The implication of the Porter-Thomas distribution is that it is essentially impossible to predict, either from systematics or from first principles, the detailed spectrum. The spectra from several resonances in ^{177}Hf (19) illustrate the difficulty. There is little resemblance between the different spectra, even of the same spin class. While systematics of the strength functions may provide reasonable expectations for the average strengths of each transition, the individual transitions behave as unpredictable statistical fluctuations.

Fortunately many measurements of the elemental thermal neutron capture spectra have been made. Recently a catalog of the prompt γ rays from thermal capture has been published and provide a convenient tool for analytical prompt γ-ray spectroscopy (20). This survey, by Lone et al., is divided into two parts: a) an energy-ordered table of capture γ's, listed along with their

intensities, element identification, capture cross section, and the two strongest γ rays from the same element.

The second part provides an element-ordered list of γ rays, with γ-ray energy uncertainties, cross sections, and intensities. Most energies are known to better than 3 keV, and many to better than 1 keV; for example, the energy uncertainties for the (7631.1, 7645.5) Fe doublet are less than 0.1 keV, the 10829.2 ^{14}N standard is known to 0.1 keV. Thus these spectra provide a unique signature for the presence of an element, provided only that a clean thermal neutron environment is present, or that the sensitivity to epithermal neutron capture is negligible.

Acknowledgements

The author is indebted for material supplied to him by Drs. Barry J. Allen, Ingvar Bergvist and W. Poenitz.

Research carried out under the auspices of the U.S. Dept. of Energy under contract no. DE-AC02-76CH00016.

References

(1) M. Goldhaber in "Neutron Capture Gamma-ray Spectroscopy", R. E. Chrien and W. R. Kane, Eds., Plenum Press, New York and London, p. 835 (1979).

(2) Fleischmann, Neutron Capture Gamma-ray Spectroscopy (1981).

(3) L. V. Groshev, A. M. Demidov, V. N. Lutsenko and V. I. Pelekhov, Proc. Intern. Conf. Peaceful Uses of Atomic Energy, 2nd Geneva Conf. 15, 138 (1958).

(4) B. B. Kinsey and G. A. Bartholomew, Can. J. Phys. 31, 537 (1953).

(5) A. M. Lane and R. G. Thomas, Rev. Mod. Phys. 30, 257 (1958).

(6) W. Heitler, Quantum Theory of Radiation, Oxford University Press (1954).

(7) J. E. Lynn, Theory of Neutron Resonance Reactions, Clarendon Press, New York, 1968.

(8) C. E. Porter and R. G. Thomas, Phys. Rev. 104, 483 (1956).

(9) A. M. Lane and J. E. Lynn, Harwell Report AERET/R2210, unpublished (1957); A. M. Lane and J. E. Lynn, Prog. Phys. Soc. (London), 70A, 557 (1957).

(10) A. A. J. Spits and J. Kopecky, Nucl. Phys. A264, 63 (1976).

(11) S. F. Mughabghab and R. E. Chrien in Neutron Capture Gamma-ray Spectroscopy, eds. R. E. Chrien and W. R. Kane, Plenum Press, New York (1979), BNL 12548.

(12) P. Axel, Phys. Rev. 126, 671 (1962).

(13) D. M. Brink, Doctoral Thesis, Oxford University, 1955.

(14) C. M. McCullagh, M. L. Stelts and R. E. Chrien, Phys. Rev. C23, 1394 (1981).

(15) M. A. Gardner and D. G. Gardner, Continued Study of the Parameterization of the E1 Gamma-ray Strength Functions, UCRL-86265, June, 1981.

(16) I. Bergqvist in "Neutron Radiative Capture", Pergamon Press, to be published (1982).

(17) C. F. Clement, A. M. Lane and J. R. Rook, Nucl. Phys. 66, 273 (1965).

(18) M. Potokar, Phys. Lett. 46B, 346 (1973).

(19) M. Stefanon and F. Corvi, Nucl. Phys. A281, 240 (1977).

(20) M. A. Lone, R. A. Leavitt and D. A. Harrison, "Prompt Gamma-rays from Thermal Neutron Capture", Atomic Data & Nuclear Data, Tables 26, #6, 511 (1981).

Figure Captions

Fig. 1 Neutron capture level scheme. Resonances excited by the (n,γ) reaction decay by γ-ray emission to lower energy states. The inelastic scattering channel opens up where the neutron energy in the center-of-mass exceeds the energy of the first excited state in the target nucleus.

Fig. 2 Thermal neutron source fluxes as a function of time.

Fig. 3 Resolutions available from bent crystal and germanium diode detectors.

Fig. 4 Schematic representation of non-resonant and resonant neutron capture. Two-body interactions excite valence, doorway, and higher order particle-hole configurations. Radiative decay can occur from all components of the long-lived resonance state.

Fig. 5 Thermal capture γ-ray spectrum in Sm. The magnetic spectrometer can resolve only the high energy primary transitions and low energy cascade transitions. Note the ordinate is the energy weighted intensity $\nu(E_\gamma)\cdot E_\gamma$.

Fig. 6 Comparison of theoretical and experimental partial capture cross sections at thermal energy for ^{130}Te. Only p-wave final states are shown.

Fig. 7 Schematic representation of the energy dependence of reduced partial radiation widths. The E_γ^5 rule, applicable only in the threshold region, is observed for resonance averaged γ-ray transitions in ^{196}Pt.

Fig. 8 Mass dependence of (a) E1 and (b) M1 transitions averaged over discrete resonances in (n,γ), (γ,n) and (γ,γ') reactions. Predictions of the giant dipole resonance model for E1 transitions (dashed line) are compared with the unweighted average (solid line).

Fig. 9 Primary γ-ray intensities for final states in the reaction $^{239}Ru(n,\gamma)^{240}Pu$. Positive parity states are denoted by x, +; negative parity states by Δ, $\square$, 0. Closed circles represent states of unassigned parity.

Fig. 10 Predicted shapes for the semidirect, σ^{sd}, and direct-semidirect, σ^{dsd}, cross sections of $^{208}Pb(n,\gamma)^{209}Pb$.

Fig. 11 Gamma-ray spectra from $^{208}Pb(n,\gamma)^{209}Pb$ at various neutron energies [Ber 72]. The solid curves represent spectra calculated from the semidirect model.

Fig. 12 Cross sections for γ-ray transitions to single-particle states of ^{209}Pb. The curves are direct-semidirect cross sections calculated with a surface-peaked (solid lines) and with a complex coupling function (dashed lines).

Fig. 13 Chi-square distribution for ν = 1,3,10 and ∞. The variance of the distribution is inversely proportional to the ν, the number of degrees of freedom.

Fig. 14 Gamma-ray spectra obtained in different resonances of the $^{177}Hf(n,\gamma)$ reaction.

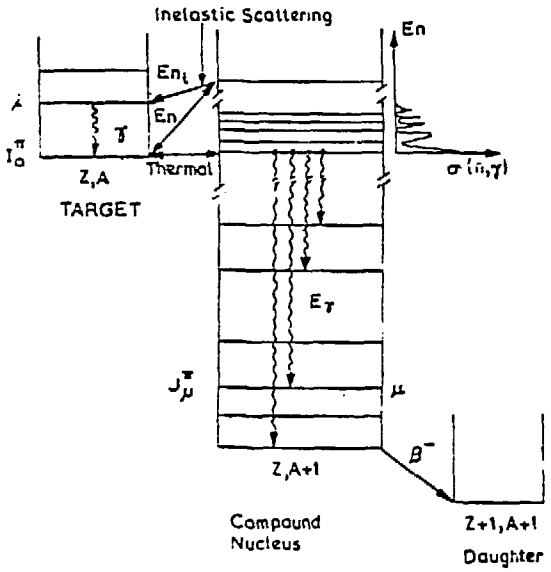
Inelastic Scattering
En
En_i
En
γ
I_o^π
Thermal
$\sigma(n,\gamma)$
Z,A
TARGET
E_γ
J_μ^π
μ
β^-
Z,A+1
Compound Nucleus
Z+1,A+1
Daughter

Fig. 1

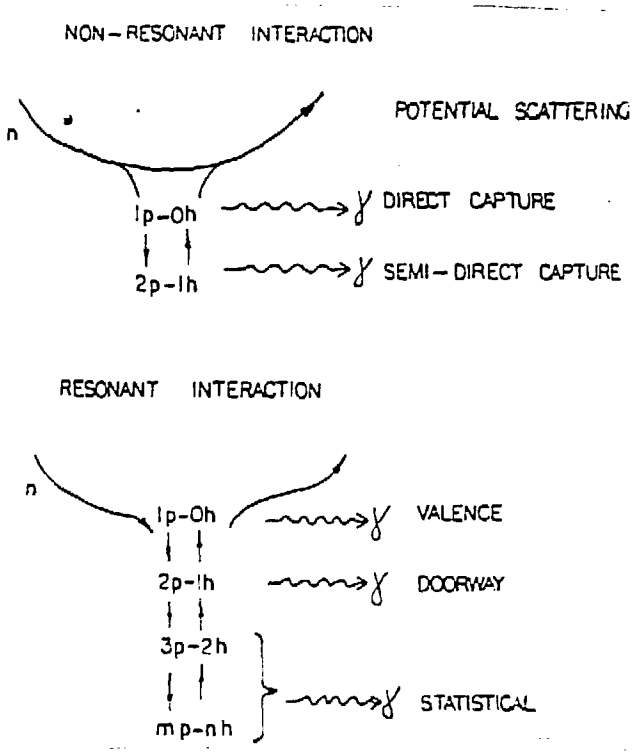
NON – RESONANT INTERACTION
n
POTENTIAL SCATTERING
1p-0h
γ DIRECT CAPTURE
2p-1h
γ SEMI – DIRECT CAPTURE
RESONANT INTERACTION
n
1p-0h
γ VALENCE
2p-1h
γ DOORWAY
3p-2h
mp-nh
γ STATISTICAL

Fig. 4

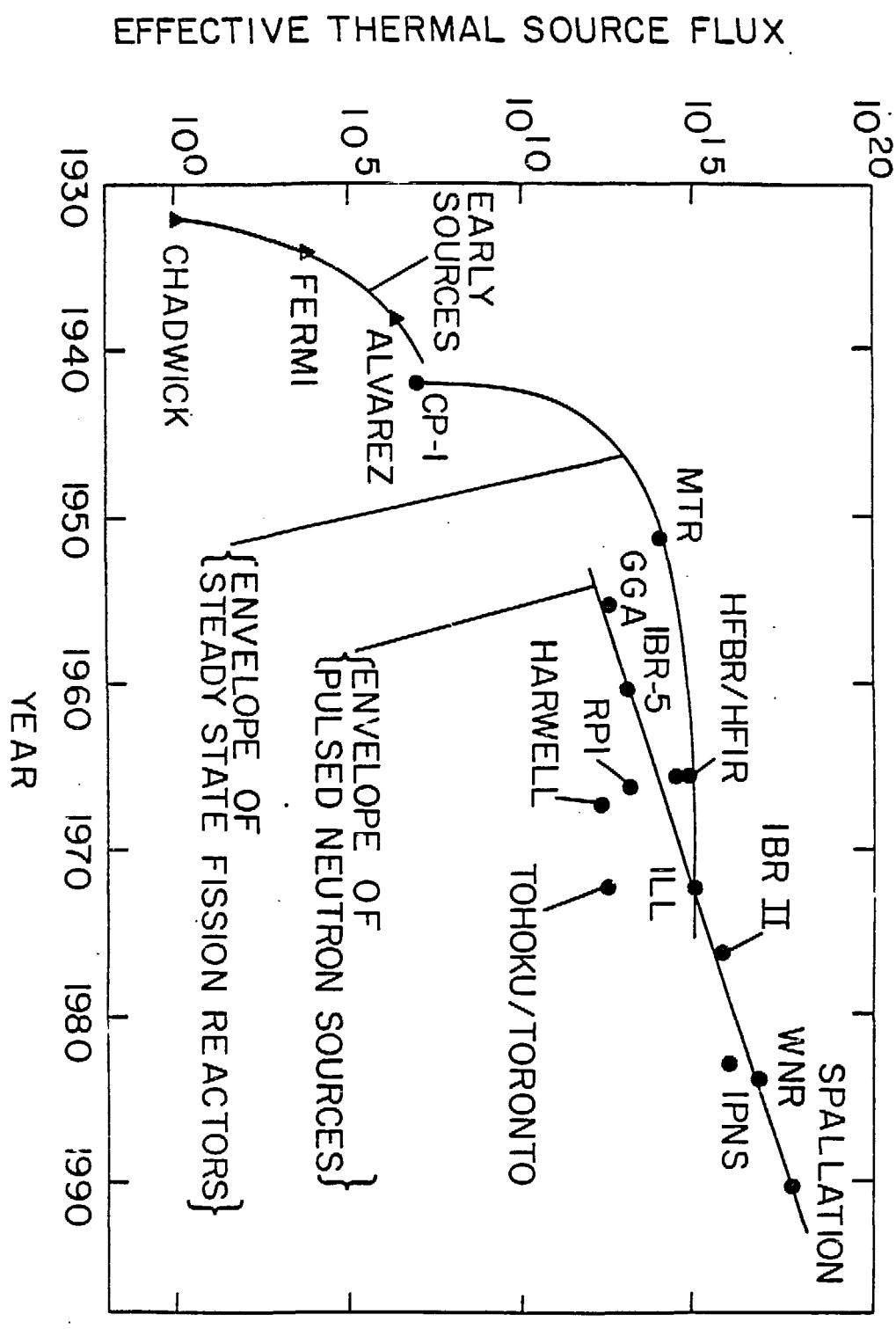
EFFECTIVE THERMAL SOURCE FLUX
10^{20}
10^{15}
10^{10}
10^{5}
10^{0}
1930
1940
1950
1960
1970
1980
1990
YEAR
CHADWICK
FERMI
ALVAREZ
EARLY SOURCES
CP-1
MTR
GGA
IBR-5
HFBR/HFIR
RPI
HARWELL
ILL
IBR II
TOHOKU/TORONTO
SPALLATION
WNR
IPNS
ENVELOPE OF STEADY STATE FISSION REACTORS
ENVELOPE OF PULSED NEUTRON SOURCES

Fig. 2

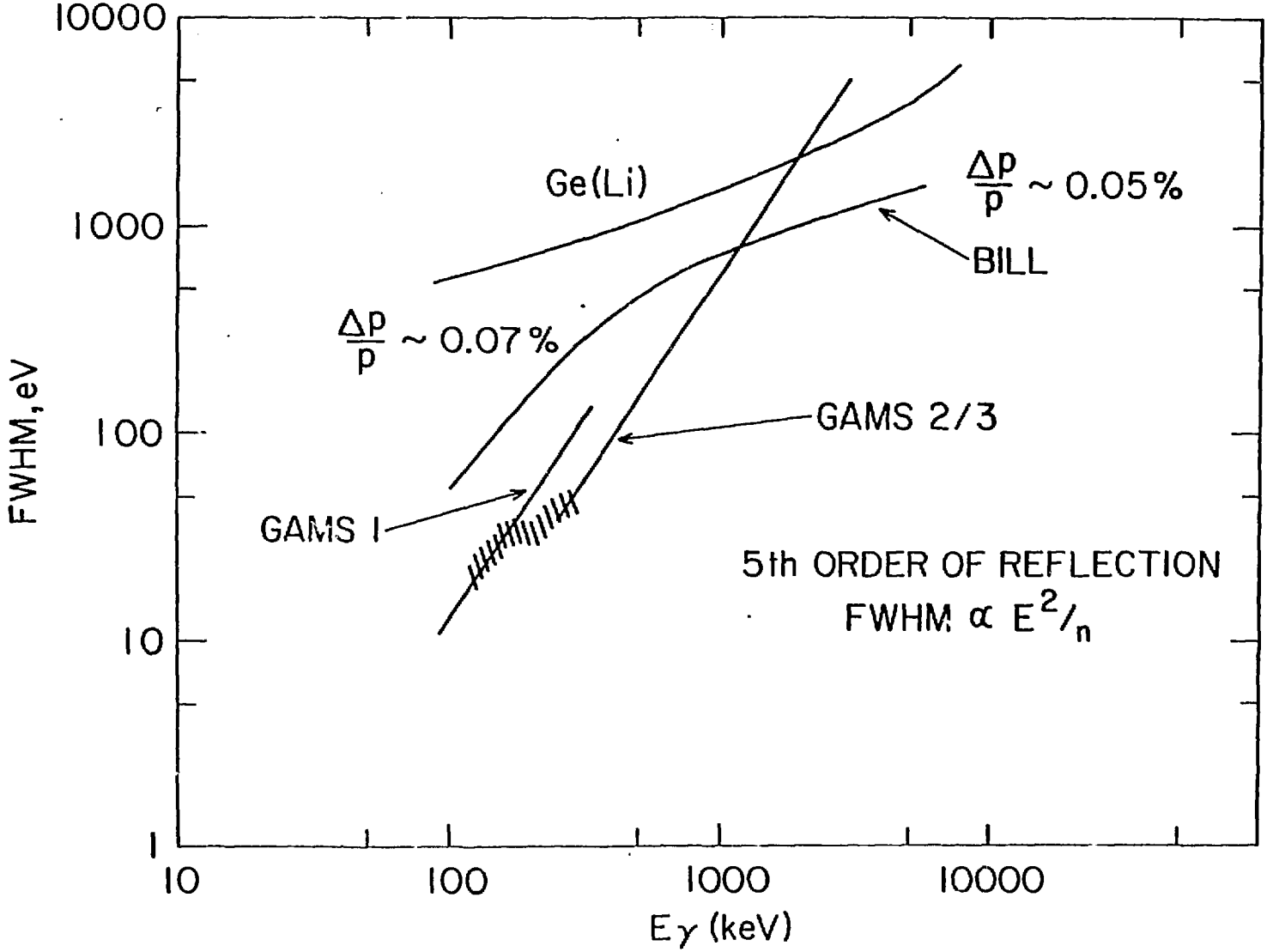
10000
1000
100
10
1
FWHM, eV
10
100
1000
10000
Eγ (keV)
Ge(Li)
ΔP/P ~ 0.05%
BILL
ΔP/P ~ 0.07%
GAMS 2/3
GAMS 1
5th ORDER OF REFLECTION
FWHM α E²/n

Fig. 3

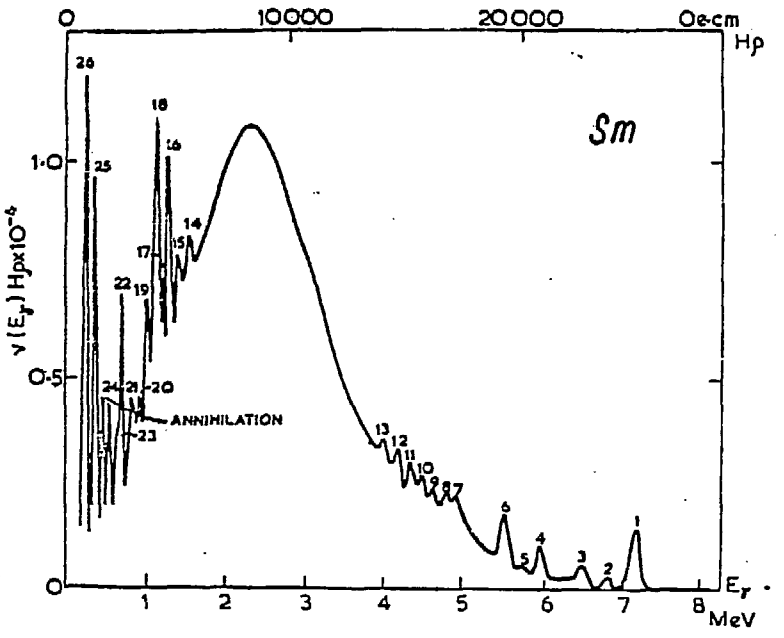
0
10000
20000
Oe-cm
Hρ
Sm
1·0
0·5
0
y(Eγ) Hρx10⁻⁴
ANNIHILATION
1
2
3
4
5
6
7
8
MeV
Eγ

Fig. 5

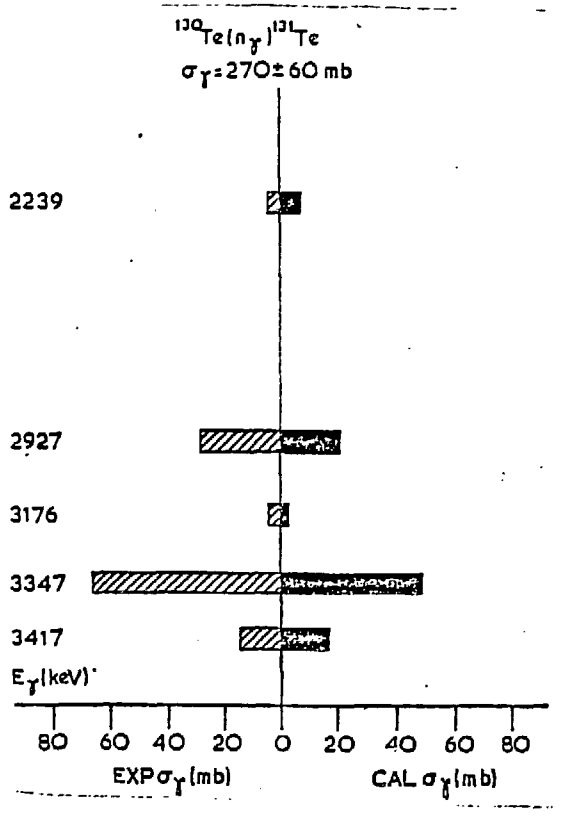
¹³⁰Te(nγ)¹³¹Te
σγ=270±60 mb
2239
2927
3176
3347
3417
Eγ(keV)
80
60
40
20
0
20
40
60
80
EXP σγ(mb)
CAL σγ(mb)

Fig. 6

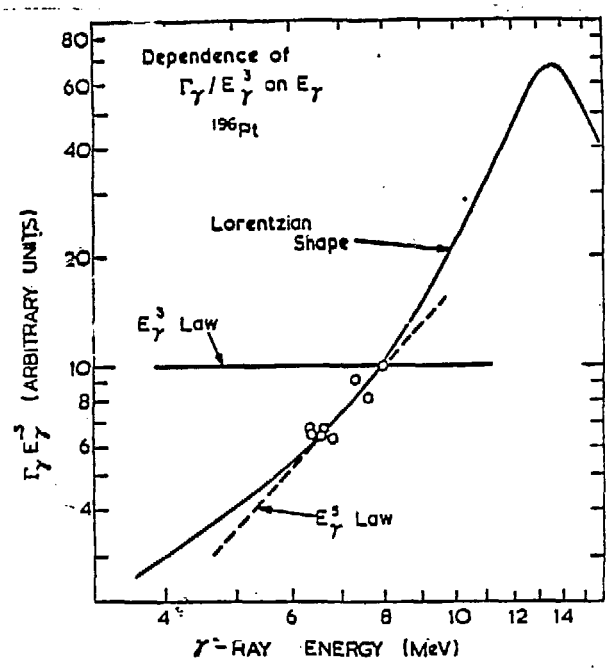
Dependence of
$\Gamma_\gamma / E_\gamma^3$ on E_γ
^{196}Pt
Lorentzian Shape
E_γ^3 Law
E_γ^3 Law
$\Gamma_\gamma E_\gamma^{-3}$ (ARBITRARY UNITS)
γ-RAY ENERGY (MeV)
80
60
40
20
10
8
6
4
4
6
8
10
12
14

Fig. 7

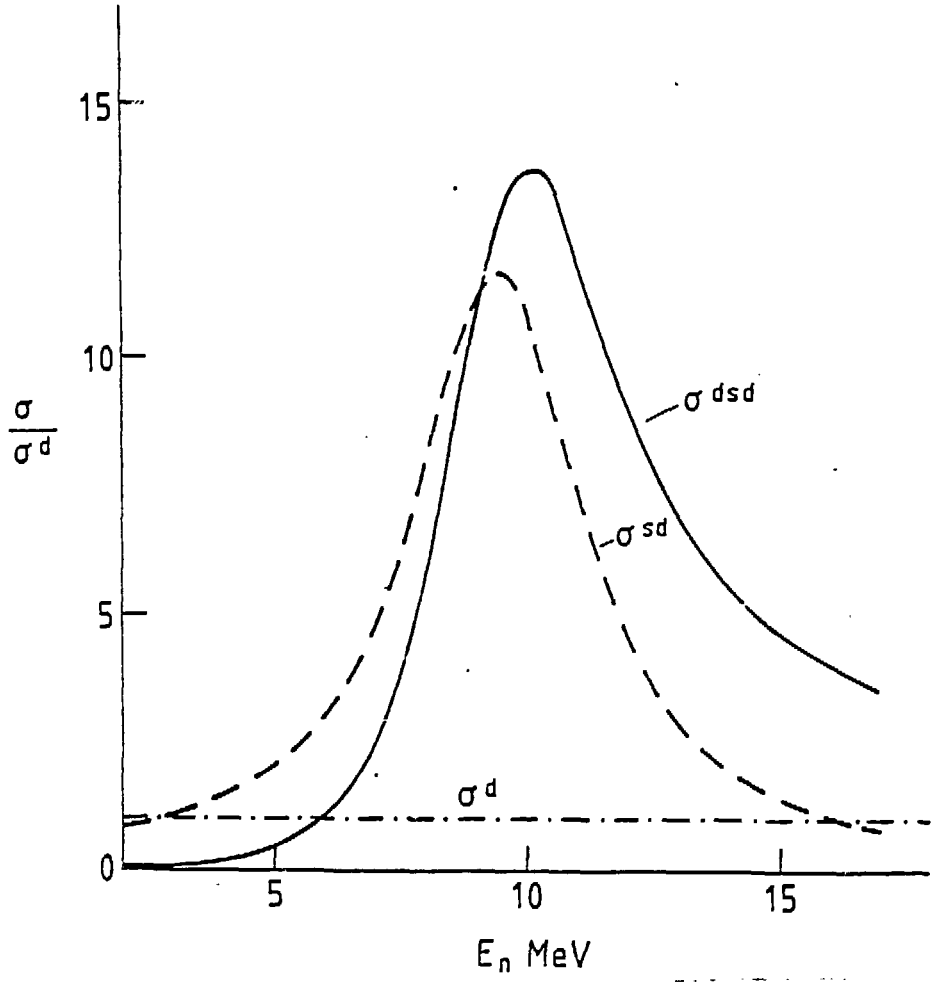
$\frac{\sigma}{\sigma_d}$
σ_{dsd}
σ_{sd}
σ_d
E_n MeV
15
10
5
0
5
10
15

Fig. 10

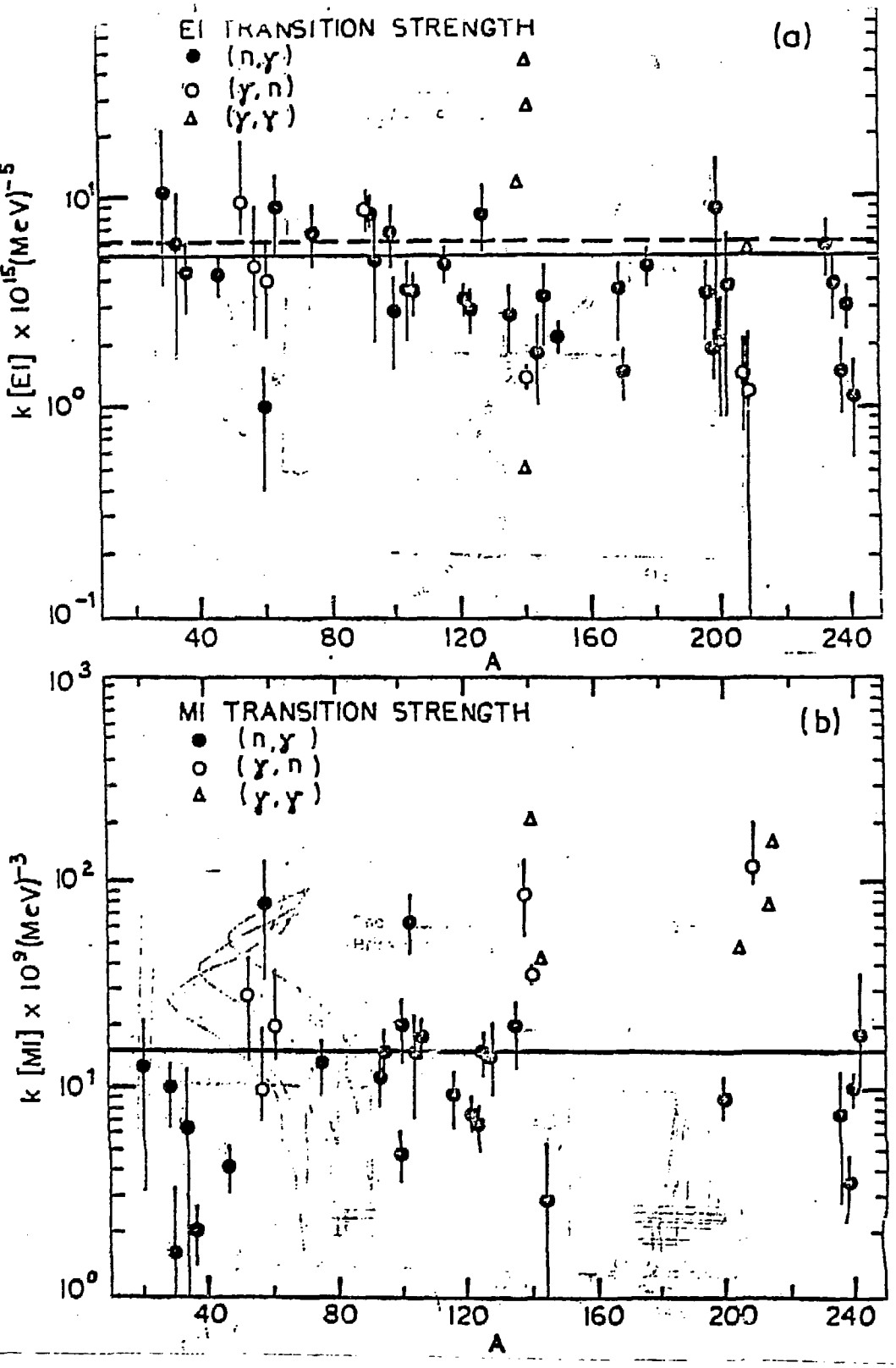
E1 TRANSITION STRENGTH
(a)
(n,γ)
(γ,n)
(γ,γ)
k [E1] x 10^15 (MeV)^-5
A
M1 TRANSITION STRENGTH
(b)
(n,γ)
(γ,n)
(γ,γ)
k [M1] x 10^9 (MeV)^-3
A

Fig. 8

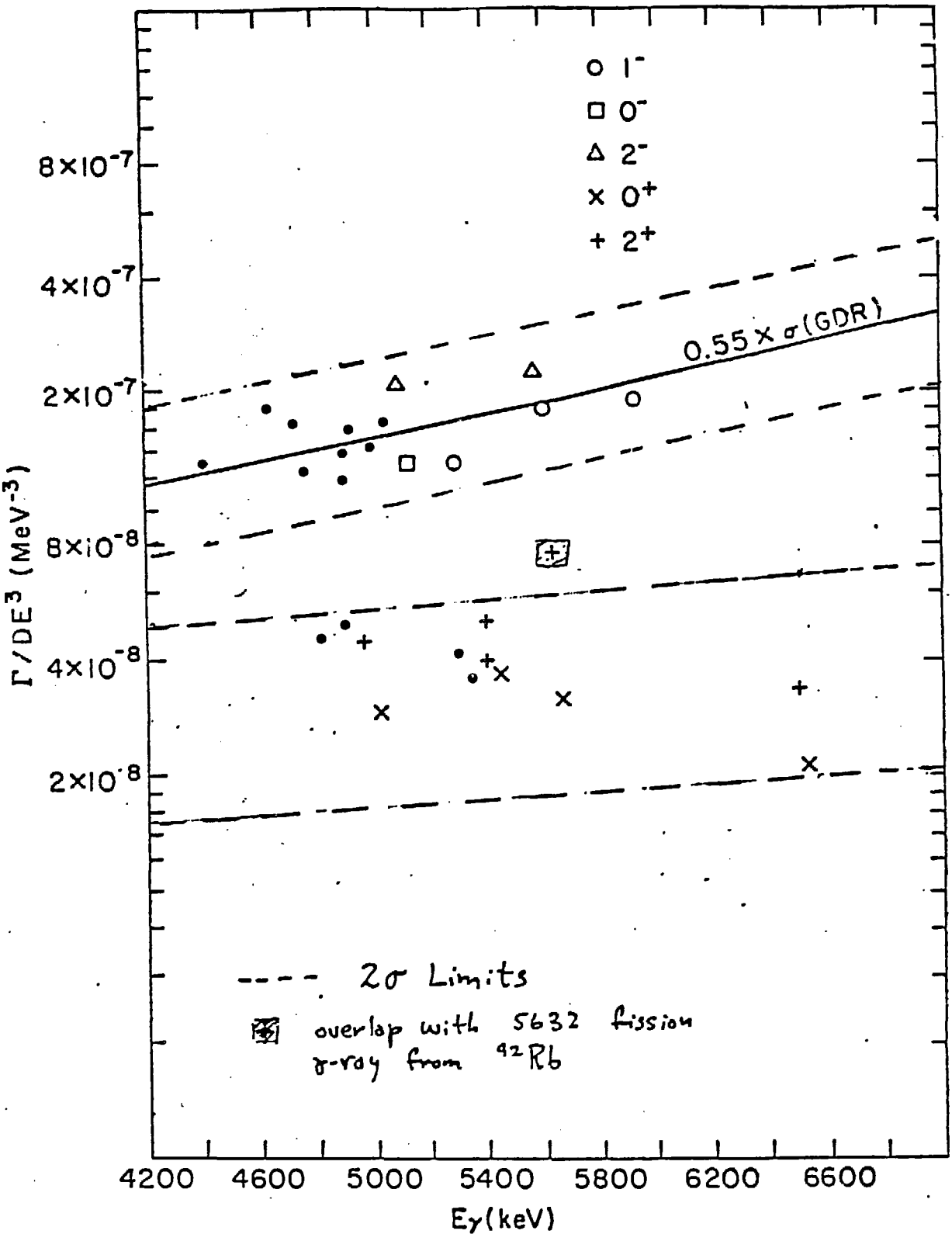
o 1⁻
□ 0⁻
Δ 2⁻
× 0⁺
+ 2⁺
0.55 × σ(GDR)
8×10⁻⁷
4×10⁻⁷
2×10⁻⁷
8×10⁻⁸
4×10⁻⁸
2×10⁻⁸
Γ/DE³ (MeV⁻³)
---- 2σ Limits
overlap with 5632 fission γ-ray from ⁹²Rb
4200
4600
5000
5400
5800
6200
6600
Eγ(keV)

Fig. 9

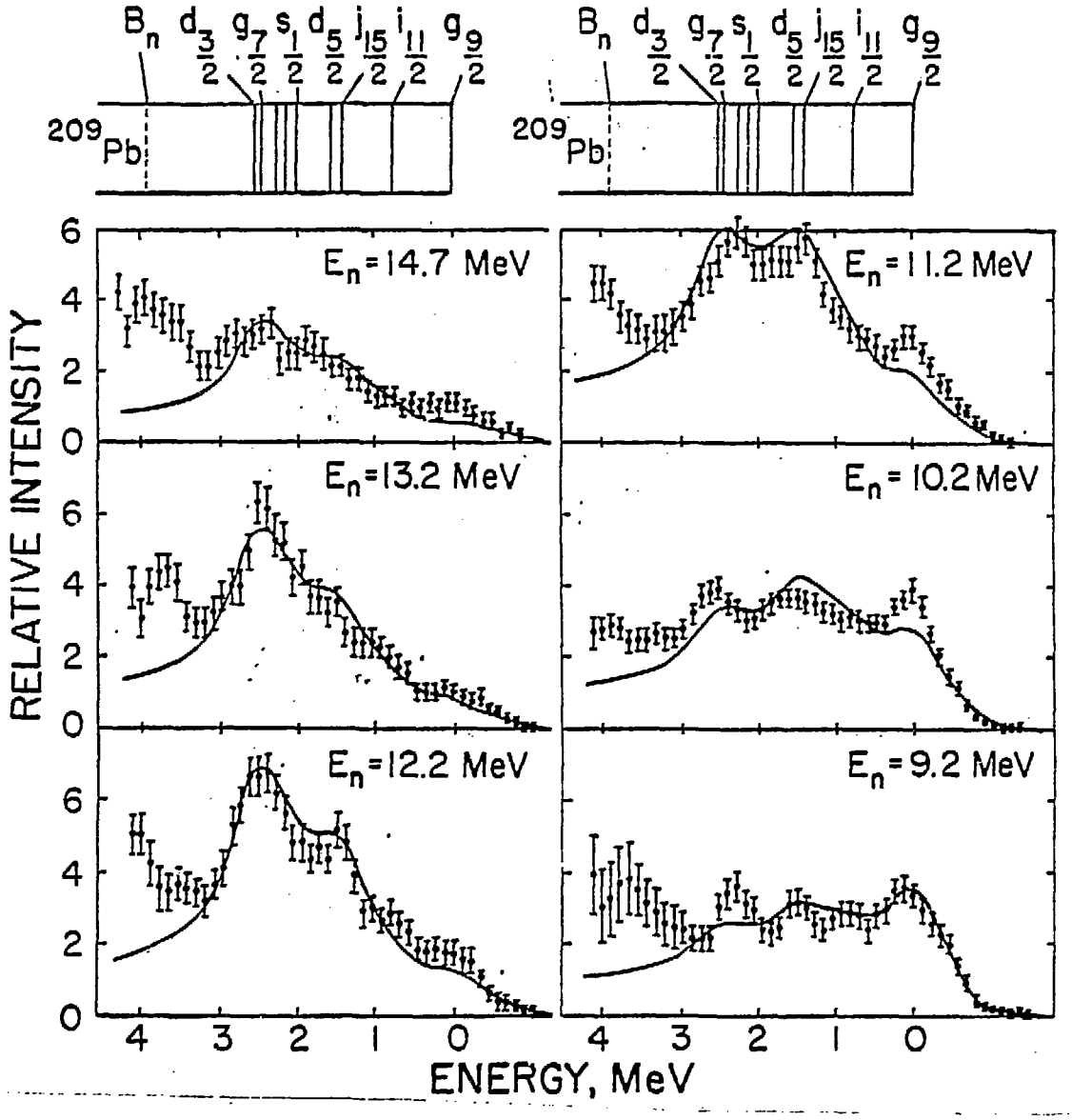
B_n d_3/2 g_7/2 s_1/2 d_5/2 j_15/2 i_11/2 g_9/2
209Pb
B_n d_3/2 g_7/2 s_1/2 d_5/2 j_15/2 i_11/2 g_9/2
209Pb
RELATIVE INTENSITY
E_n = 14.7 MeV
E_n = 11.2 MeV
E_n = 13.2 MeV
E_n = 10.2 MeV
E_n = 12.2 MeV
E_n = 9.2 MeV
0
2
4
6
4 3 2 1 0
ENERGY, MeV

Fig. 11

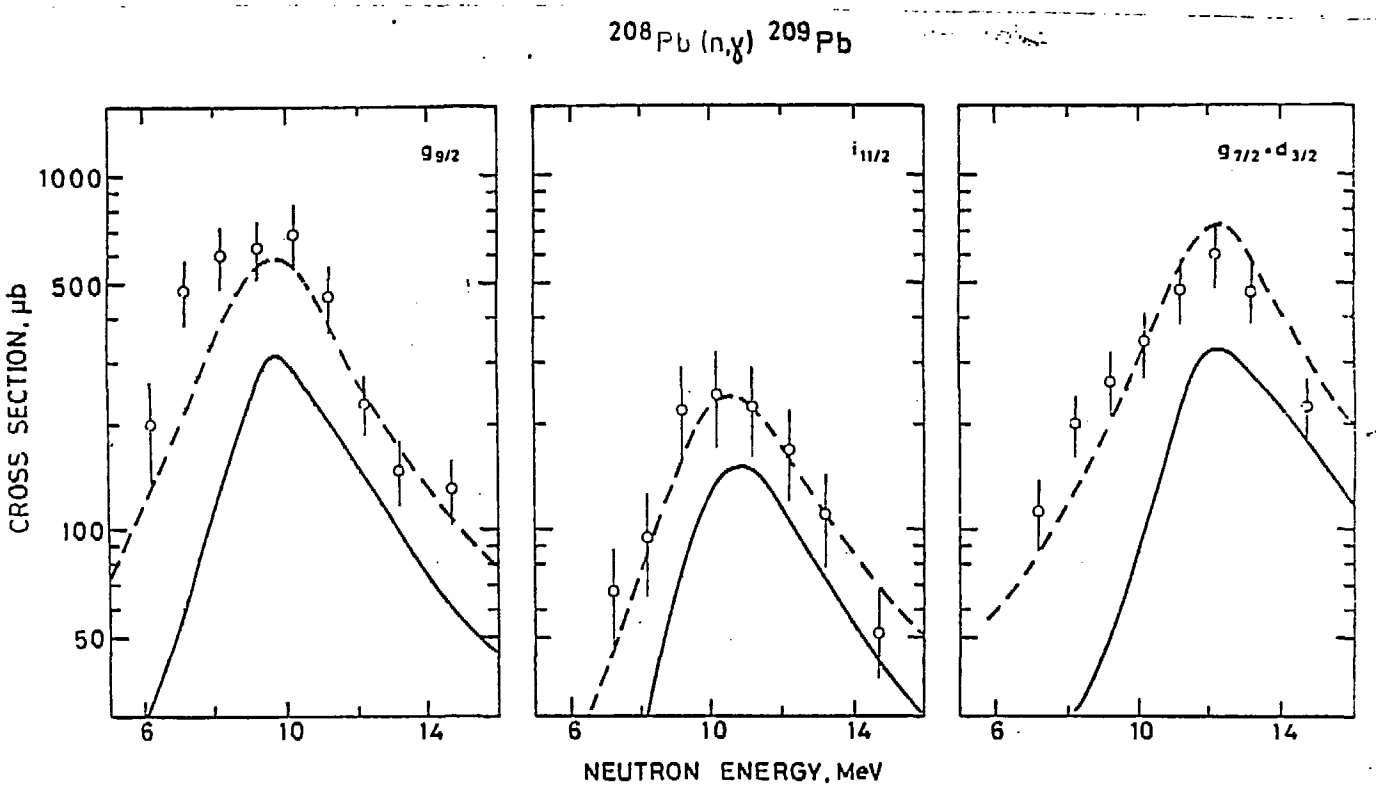
$^{208}Pb\ (n,\gamma)\ ^{209}Pb$
$g_{9/2}$
$i_{11/2}$
$g_{7/2}+d_{3/2}$
1000
500
100
50
CROSS SECTION, μb
6
10
14
NEUTRON ENERGY, MeV

Fig. 12

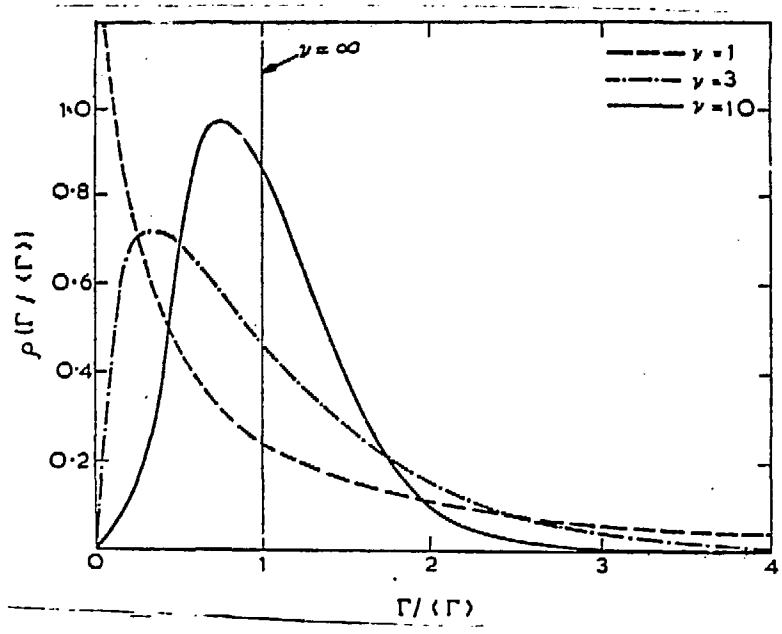
$\nu = \infty$
$\nu = 1$
$\nu = 3$
$\nu = 10$
1·0
0·8
0·6
0·4
0·2
$\rho(\Gamma / \langle\Gamma\rangle)$
0
1
2
3
4
$\Gamma / \langle\Gamma\rangle$

Fig. 13

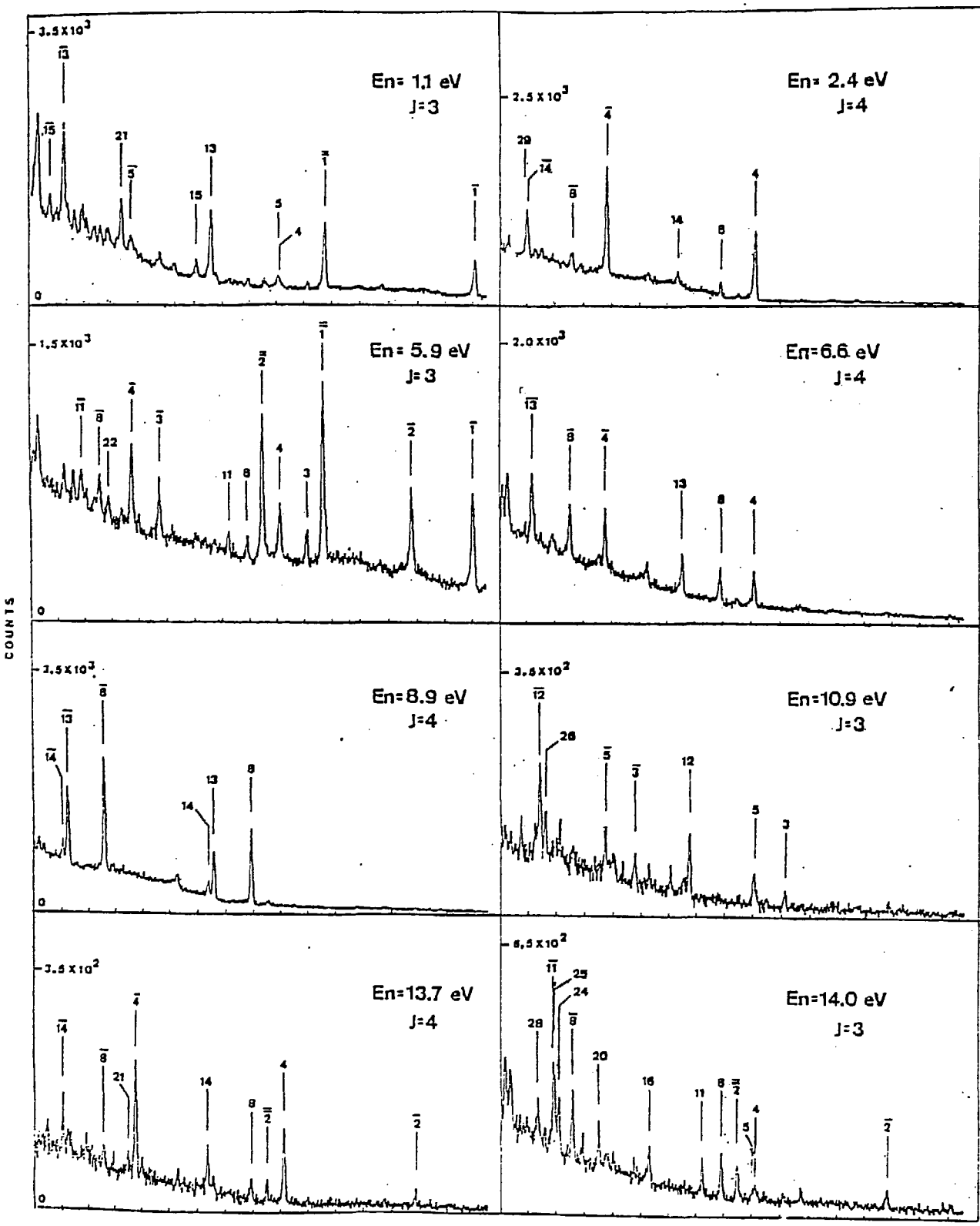
COUNTS
En= 1.1 eV
J=3
En= 2.4 eV
J=4
En= 5.9 eV
J= 3
En=6.6 eV
J=4
En=8.9 eV
J=4
En=10.9 eV
J=3
En=13.7 eV
J=4
En=14.0 eV
J=3

Fig. 14